Chapter 4

ELECTRONIC STRUCTURES OF GROUP 9 METALLOCORROLES WITH AXIAL AMMINES

During the summer of 2009, an undergraduate student named Scarlett, from Chi-Ming Che's group at the University of Hong Kong, came to work with me doing DFT calculations on some iridium corrole complexes. Along with a postdoctoral student from Bill Goddard's group named Smith, who has significantly more experience with computational chemistry than I do, Scarlett ran geometry optimizations and single-point energy calculations on a variety of hypothetical corrole complexes. I wanted to see what theory had to say about the results I detailed previously in Chapter 2 of this work, so we ran calculations on Co(III), Rh(III), and Ir(III) complexes of tpfc (as well as analogous complexes of the hypothetical, and less computationally intensive, macrocycle tfc) and their one-electron oxidized forms.

The calculations, which were performed in the absence of explicitly included spin-orbit coupling terms, produced ground states for all three cations in which the highest-lying SOMO is localized largely on the corrole, with negligible metal character. Later, more sophisticated computational results will be discussed later in the thesis, and suggest significant spin on the metal in the case of iridium. However, those calculations include (and examine) parameters with which we were not concerned at the time we did the work presented in this chapter, and the inspiration for performing them stemmed from the computational work discussed below.

Electronic Structures of Group 9 Metallocorroles with Axial Ammines

Reproduced with permission from: Sijia S. Dong, Robert J. Nielsen, Joshua H. Palmer, Harry B. Gray, Zeev Gross, Siddharth Dasgupta, and William A. Goddard III. *Inorg. Chem.*, **2011**, *50* (3), pp 764–770.

Abstract

The electronic structures of metallocorroles (tpfc)M(NH_3)$_2$ [**1-M(NH_3)$_2$**] and (tfc)M(NH_3)$_2$ [**1f-M(NH_3)$_2$**] (tpfc is the trianion of 5,10,15-(tris)pentafluorophenylcorrole, tfc is the trianion of 5,10,15-trifluorocorrole, and M = Co, Rh, Ir) have been computed using first principles quantum mechanics [B3LYP flavor of Density Functional Theory (DFT) with Poisson-Boltzmann continuum solvation]. The geometry was optimized for both the neutral systems (formal M^{III} oxidation state) and the one-electron oxidized systems (formally M^{IV}). As expected, the M^{III} systems have a closed shell d^6 configuration; for all three metals, the one-electron oxidation was calculated to occur from a ligand-based orbital (HOMO of B_1 symmetry). The ground state of the formal M^{IV} system has M^{III}-Cπ character, indicating that the metal remains d^6, with the hole in the corrole π system. As a result the calculated $M^{IV/III}$ reduction potentials are quite similar (0.64, 0.67, and 0.56 V vs. SCE for M = Ir, Rh and Co, respectively), whereas the differences would have been large for purely metal-based oxidations. Vertically excited states with substantial metal character are well separated from the ground state in one-electron-oxidized cobalt (0.27 eV) and rhodium (0.24 eV) corroles, but become closer in energy in the iridium (0.15 eV) analogues. The exact splittings depend on the chosen functional and vary by ~ 0.1 eV.

Introduction

Understanding the factors that determine the stability and reactivity of metal complexes in high oxidation states could greatly facilitate the design of catalysts for substrate oxidation reactions.[1] A major problem that must be addressed is that the ligands themselves often undergo redox changes during catalysis.[2,3,4] Such non-innocent ligand behavior is a hallmark of oxidative catalytic cycles of heme enzymes, where a highly reactive intermediate (Compound I) formed by two-electron oxidation of an iron(III) precursor is better described as an oxoiron(IV) ligand radical than as an iron(V) complex.[5] Depending on the particular enzyme, one unpaired electron is located on either an orbital of the chelating porphyrin or on a nearby amino acid residue.[6] Importantly, advances in synthesis, together with high level spectroscopy and theory, have shed new light on these and related issues, with surprising findings in certain cases: for example, the likelihood of a role for electronic excited-state coupling in promoting catalytic hydroxylations by heme and nonheme-iron enzymes.[7]

The recent explosive growth in corrole chemistry has provided many new examples that challenge current views of the electronic structures of complexes containing non-innocent ligands.[8] Although corroles (both metal-free and in complexes with non-redox-active elements) are prone to oxidation,[9] it is well established that they stabilize transition metals in unusually high oxidation states.[10] In some cases, non-innocent behavior has made it particularly difficult to assign metal and ligand oxidation states, as in five-coordinate (chloro)iron corroles, where a combination of spectroscopy and DFT calculations has established that metal- and corrole-based orbitals are strongly coupled.[11]

Our recent experimental work has highlighted the need to develop electronic structural descriptions of analogous 3d-4d-5d Group 9 metallocorroles, as the successful syntheses of five- and six-coordinate iridium(III) corroles completed a very rare isostructural 3d (Co^{III}), 4d (Rh^{III}), and 5d (Ir^{III}) series.[12] Surprisingly, the reduction potentials show very little variation among the three corroles, while EPR results suggest a shift from corrole- to metal-centered oxidation in moving from 3d and 4d to 5d complexes. These findings have led us to attempt full electronic structural elucidation of Group 9 metallocorroles by computational methods.

Third-row transition metal corroles are rare[13] (in addition to Ir, one Re complex has been reported).[14] Among elements in the periodic table, only those in Group 9 feature corrole complexes for all three metals. The structures and reactivity patterns of the Group 9 metallocorroles have been characterized previously using a battery of experimental techniques, and we believe that computational analyses of their electronic structures will allow us to refine our interpretations of the properties of these interesting molecules. In particular, we do not have a satisfactory explanation for the small differences in $Co^{IV/III}$, $Rh^{IV/III}$, and $Ir^{IV/III}$ reduction potentials. And another puzzle is the greatly enhanced metal character indicated by EPR spectra in going from "Co^{IV}" and "Rh^{IV}" to "Ir^{IV}".

We have employed density functional theory (DFT)[15] as the method of choice for determination of metallocorrole electronic structures. The structural parameters of **1-Ir(NH$_3$)$_2$** from the calculations are consistent with those obtained from X-ray diffraction crystallographic measurements on **1-Ir(tma)$_2$** and **1-Ir(py)$_2$** (tma = trimethylamine and py = pyridine).[12,13] Calculations were made of the reduction potentials as well as the

electronic structures of [**1-M(NH$_3$)$_2$**]$^{0/+}$. Additionally, less computationally taxing [**1f-M(NH$_3$)$_2$**]$^{0/+}$ models were examined. Our computational results show that the very small nd (n = 3,4,5) dependence of the reduction potentials of Group 9 metallocorroles is accompanied by a marked decrease in metal orbital energies (compared with those of the corrole) in the order 3d-4d-5d.

Computational Details

All computations were conducted with the Jaguar 7.0 package (release 207),[16] applying the hybrid density functional B3LYP.[17] B3LYP has proved useful in the calculation of oxidation potentials[18] and yielded spin density distributions and excited state orderings similar to CASPT2 results for an iron-heme model.[19]

Free energies used in the calculation of oxidation potentials are equal to:

$$G = E_{el,gas} + G_{solv} + ZPE + H_{vib} - S_{vib}T$$

where $E_{el,gas}$ is the gas phase electronic energy, G_{solv} is the solvation energy of the compound in dichloromethane, ZPE is the zero-point energy of the complex, H_{vib} is the vibrational enthalpy, and S_{vib} is the vibrational entropy. The temperature was set to 298 K for all calculations.

Angular-momentum-projected nonlocal effective core potentials[20] (pseudopotentials) optimized by Hay and Wadt [21] were used to replace the core electrons. Thus, the Co, Rh, and Ir atoms were each described with 17 explicit electrons (two 5s, six 5p, plus nine (6s,5d) for neutral Ir). Geometries of the neutral and cationic complexes were optimized

and hessians for vibrational spectra were calculated in vacuum using the 2-ζ valence functions for the metals and 6-31G**[22] for all other atoms. Single point energies were then calculated using a 3-ζ contraction of the Los Alamos valence functions augmented with two f-functions[23] for metals and 6-311G**$^{++}$ for other atoms. These single point energies were used to calculate the oxidation potentials. Solvation energies were obtained at the vacuum-optimized geometries with the PBF Poisson-Boltzmann continuum solvation model[24] using default atomic radii, a dielectric constant of ε = 8.93 and probe radius of 2.33 Å to represent dichloromethane. The accuracy of this methodology has been validated in several recent reports.[18,25]

The oxidation potentials (in V) relative to the standard hydrogen electrode (SHE) were calculated using the Nernst equation

$E_{SHE} = (G_{ox}-G_{red}) / (N_{el})(23.06 \text{ kcal/mol·eV}) - 4.3V,$

where N_{el} is 1 e^-, the number of electrons removed. The absolute potential of the standard hydrogen electrode (4.3V) is derived from Tissandier et al.'s determination of the absolute solvation energy of a proton.[26] G_{ox} is the Gibbs free energy (in kcal/mol) of the oxidized form of the complex and G_{red} is that of the reduced form. The corresponding potentials relative to the saturated calomel electrode (SCE) are

$E_{SCE} = E_{SHE} – 0.24V$[27].

To simplify orbital analysis of excited states, geometries of the neutral **1-M(NH$_3$)$_2$** and **1f-M(NH$_3$)$_2$** complexes were re-optimized with C_{2v} symmetry enforced. Then, single point energy calculations using the 2-ζ basis were performed on the corresponding

"M(IV)" complexes to obtain the energies of various states with the electron taken from different orbitals of the M(III) complexes. Level-shifting was applied to aid convergence of the excited states, and the obtained states were resubmitted to the SCF procedure without level-shifting for verification. Orthogonality of excited states in our SCF approach is only guaranteed for the lowest-lying states. This is sufficient because our primary concern involves distinguishing metal-based from ligand-based oxidation in the ground states.

All doublet states used unrestricted orbitals. The spin densities and charges on the metals were also obtained through Mulliken analysis. Unless otherwise stated in the text, upper-case symmetry labels (e.g., 1^2A_2) denote excited states with the electron ionized from an orbital of the corresponding symmetry. The orbitals themselves are denoted by lower-case symmetry labels (e.g., $1a_2$). The numbering of both orbitals and states proceeds from lower to higher energy in both cases.

Results

Geometry of the Ground State. The crystal structures of known iridium corroles show that there is a quasi-twofold axis that passes through Ir and C10 (Figure 4-1). Both Ir-N(tma) bond lengths in **1-Ir(tma)$_2$** are 2.185 Å; Ir-N(pyridine) bond lengths in **1-M(py)$_2$** are 2.052 and 2.066 Å; and Ir-N(pyrrole) bond lengths range from 1.940 to 1.981 Å. The computed Ir-N(ammine) and Ir-N(pyrrole) bond lengths are, respectively, 2.112 and 1.976 to 1.996 Å, in good agreement with the crystallographic data of the aforementioned Ir(III) corroles. Dihedral angles of the pentafluorophenyl groups in vacuum-optimized structures are 66–76 degrees. The energy change caused by rotation of the

pentafluorophenyl groups away from perpendicular averages 0.03 eV, which we consider as less than the energy accuracy in computations.

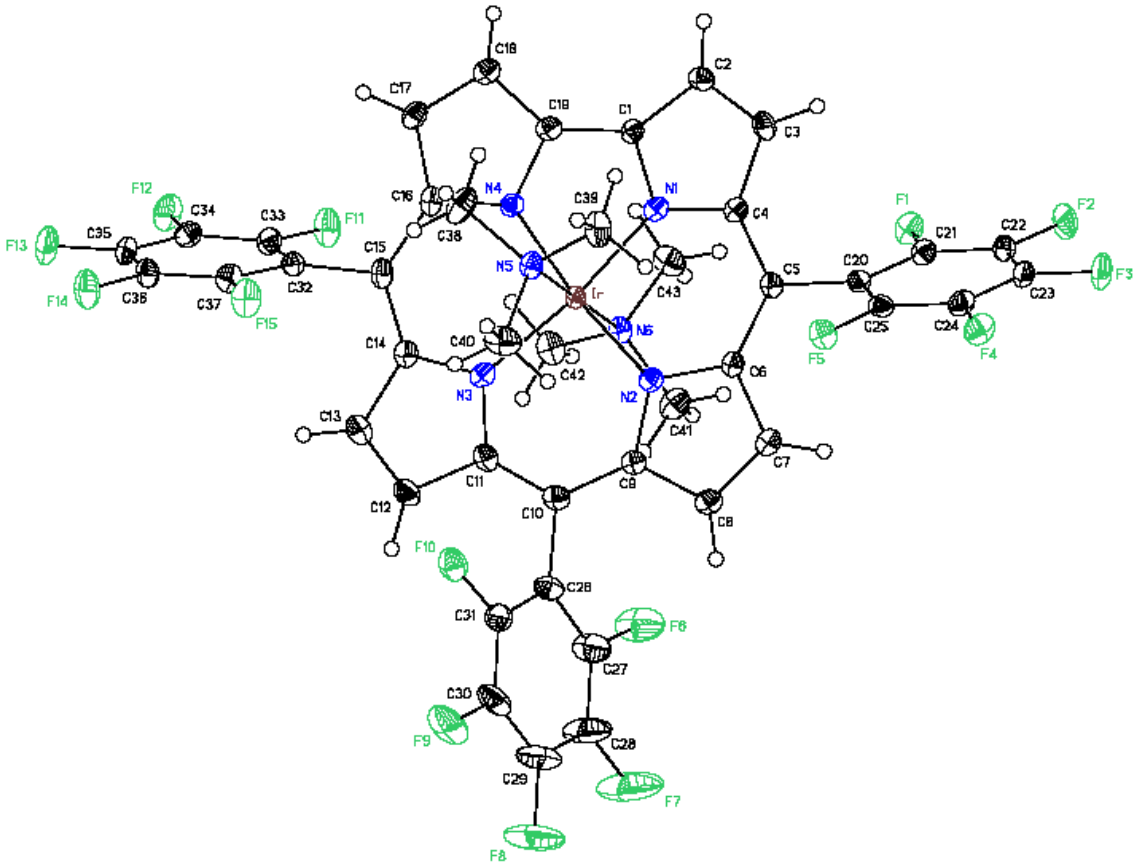

Figure 4-1: X-ray structure of **1-Ir(tma)$_2$** (structure previously published in ref. 13). Hydrogen atoms are in white, carbon atoms are in black, nitrogen atoms are in blue, fluorine atoms are in green, and iridium is in red

The computed increases in the lengths of bonds C5-C6 and C1-C19 (Table 4-1) upon removal of an electron from the neutral complexes, along with the concomitant decrease in the length of the bond C4-C5, are consistent with Ghosh's description of alternating bond length changes upon formation of a corrole-based cation radical of B_1 symmetry.[28]

Table 4-1: Key bond lengths of [**1-M(NH$_3$)$_2$**]$^{0/+}$ in angstrom, for M = Co, Rh, and Ir. All structures relaxed without symmetry with their ground state wavefunction. The row r(M-NH$_3$) corresponds to the average distance from the metal to the axial amine nitrogen atoms. The geometries were calculated in vacuum by DFT using the 2-ζ valence functions with Hay and Wadt pseudopotentials for the metals and a 6-31G** basis set for all the other atoms. The B3LYP functional was employed. [a]Indicates the change of the given bond length upon oxidation of the complex

Distance (Å)	[(tpfc)Co(NH$_3$)$_2$]^0	[(tpfc)Co(NH$_3$)$_2$]$^+$	Change[a]	[(tpfc)Rh(NH$_3$)$_2$]^0	[(tpfc)Rh(NH$_3$)$_2$]$^+$	Change[a]	[(tpfc)Ir(NH$_3$)$_2$]^0	[(tpfc)Ir(NH$_3$)$_2$]$^+$	Change[a]
r(M-N5)	1.988	1.995	0.007	2.107	2.114	0.007	2.112	2.119	0.007
r(M-N6)	1.987	1.992	0.005	2.108	2.116	0.008	2.112	2.120	0.008
r(M-NH$_3$)	1.988	1.994	0.006	2.108	2.115	0.007	2.112	2.120	0.008
r(M-N1)	1.887	1.888	0.001	1.967	1.968	0.001	1.976	1.976	0.000
r(M-N2)	1.916	1.913	-0.003	1.993	1.991	-0.002	1.997	1.996	-0.001
r(N1-C1)	1.370	1.356	-0.014	1.369	1.355	-0.014	1.371	1.356	-0.015
r(N1-C4)	1.360	1.371	0.011	1.356	1.365	0.009	1.360	1.367	0.007
r(N2-C6)	1.386	1.373	-0.013	1.380	1.368	-0.012	1.383	1.370	-0.013
r(N2-C9)	1.371	1.375	0.004	1.365	1.369	0.004	1.368	1.371	0.003
r(C1-C19)	1.425	1.442	0.017	1.446	1.466	0.020	1.450	1.471	0.021
r(C4-C5)	1.414	1.401	-0.013	1.428	1.414	-0.014	1.429	1.415	-0.014
r(C5-C6)	1.408	1.431	0.023	1.422	1.447	0.025	1.425	1.449	0.024
r(C9-C10)	1.410	1.414	-0.004	1.424	1.428	-0.004	1.426	1.429	-0.003

Wavefunction Character of the Ground State. As expected, the ground state of (tpfc)Ir(NH$_3$)$_2$ has six electrons in the t_{2g}-derived d orbitals (d_{xy}, d_{xz}, d_{yz}) with a closed-shell corrole π-system (Figure 4-2). However for the ground state of [(tpfc)Ir(NH$_3$)$_2$]$^+$, we find that the d^6 configuration on Ir remains intact while the $2b_1$ orbital of the corrole is singly occupied. There is effectively no spin density on the metal, and the atomic charge of Ir from Mulliken population analysis remains essentially constant (0.87 to 0.89). Thus this system, which is formally Ir(IV), is better described as Ir(III)-Cπ where Cπ denotes a hole in the highest HOMO of the corrole. However, experimental EPR data from other iridium corroles,[12] showing significant anisotropy in the g tensor for the oxidized species [(tpfc)Ir(tma)$_2$]$^+$ and [(tpfc)Ir(py)$_2$]$^+$, demonstrate that there is some degree of iridium d

orbital character mixed into the ground state of the oxidized iridium corroles. Co and Rh are similar as shown in the supporting information.

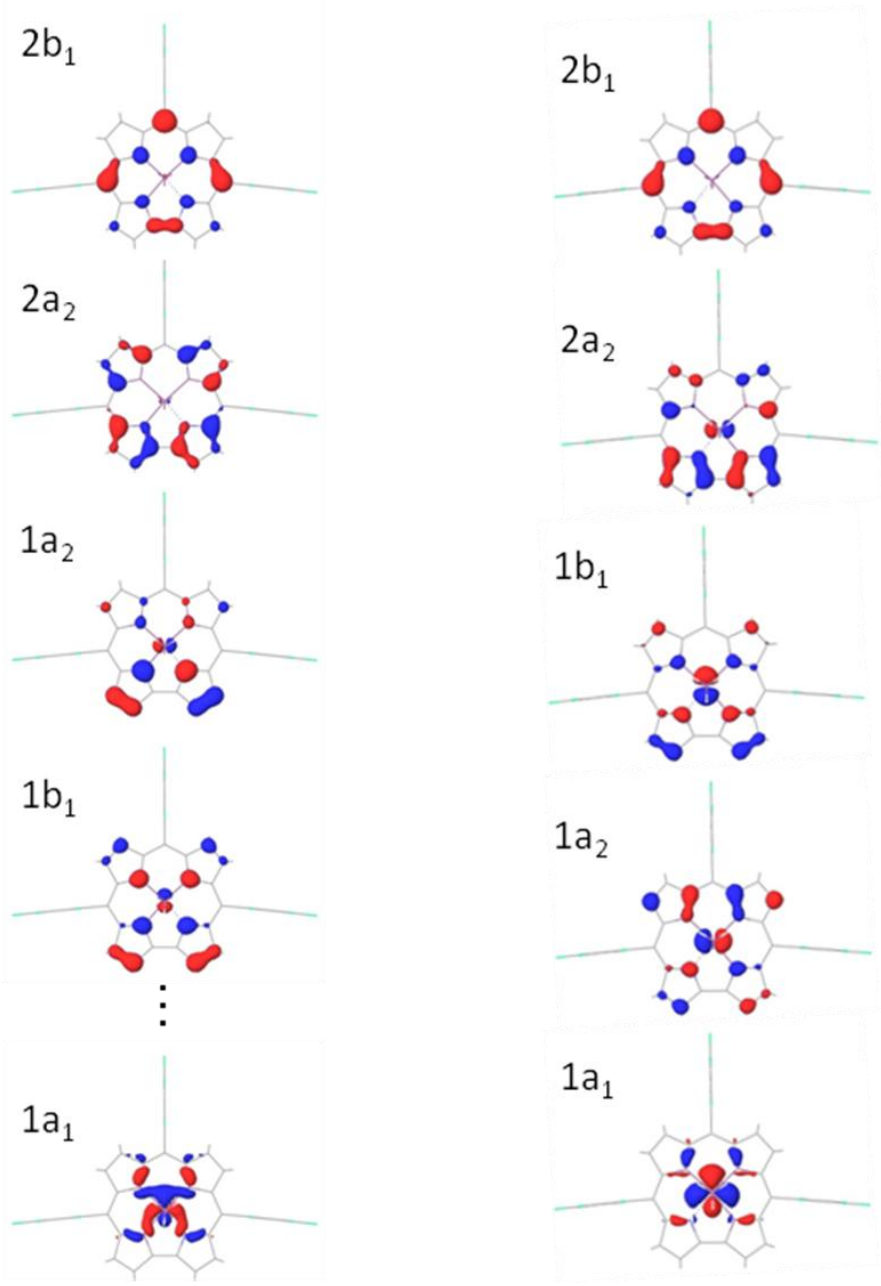

Figure 4-2: Molecular orbital (MO) surfaces (isovalue = 0.05 a. u.) of **1-M(NH$_3$)$_2$**, where M = Rh (left, Co is similar) or Ir (right). The topmost MO is the HOMO, which is followed by HOMO-1, and so on. 1a$_1$ is HOMO-13 when M = Rh, HOMO-14 when M = Co, and HOMO-4 when M = Ir. The omitted orbitals on the left side are corrole-based. The geometries were calculated in vacuum by DFT using the 2-ζ valence functions with Hay and Wadt pseudopotentials for the metals and a 6-31G** basis set for all the other atoms. The B3LYP functional was employed.

The relative energies as well as the metal spin densities of [**1-M(NH$_3$)$_2$**]$^+$ excited states are compared in Table 4-2. The spin density plots in Figure 4-3 show that the higher-energy excited states for each metal, particularly for iridium, contain significant metal character. Typically, two imaginary frequencies with magnitude less than 10 cm^{-1} were obtained when no symmetry was applied to the tpfc complexes. These frequencies generally involve motions of the C_6F_5 groups on the corrole rings and are not important in defining metal-based transitions. For the purposes of calculating thermodynamic contributions, imaginary frequencies were excluded. Symmetry constraints changed the combination modes that have imaginary frequencies, and increased the number of the imaginary frequencies to three with each lying a bit over 20 cm^{-1}. Upon oxidation, the imaginary frequencies tend to be of smaller magnitude or even become non-imaginary, but the changes show no universal trend.

Although the pentafluorophenyl group (C_6F_5) is the meso substituent in experimentally characterized compounds, the model [**1f-M(NH$_3$)$_2$**]$^+$ complexes also were examined in order to reduce computation times and control for computational artifacts arising from the presence of imaginary frequencies in the tpfc complexes. Parameters for the tfc complexes are set out in Table 4-3; and spin density surfaces and energy levels of these complexes are shown in Figure 4-4.

Table 4-2: Spin densities and energies of the excited states of the tpfc complexes. The symmetry label of the state is the symmetry of the orbital from which the electron has been ionized. For Rh and Co, other states lying between 2^2B_1 and 1^2A_1 but having the unpaired electron in corrole-based orbitals were omitted in order to include the metal-dominated 1^2A_1. The calculations were conducted in vacuum by DFT using the 2-ζ valence functions with Hay and Wadt pseudopotentials for the metals and 6-31G** basis set for all the other atoms. The B3LYP functional was employed. [a]Energy of the state in question minus that of the lowest energy ionized state of the same compound. [b]Spin given in total unpaired electrons

$[(tpfc)M(NH_3)_2]^+$	**M = Co**		**M = Rh**		**M = Ir**	
State	**Relative energy (eV)[a]**	***Metal spin density*[b]**	**Relative energy (eV) [a]**	***Metal spin density*[b]**	**Relative energy (eV) [a]**	***Metal spin density*[b]**
1^2B_1	0.00	*-0.02*	0.00	*-0.01*	0.00	*-0.01*
1^2A_2	0.27	*0.00*	0.24	*0.02*	0.15	*0.07*
2^2A_2	1.63	*0.10*	1.23	*0.21*	0.59	*0.08*
2^2B_1	1.71	*0.12*	1.27	*0.24*	0.86	*0.38*
1^2A_1	2.74	*1.13*	2.71	*0.75*	2.06	*0.89*

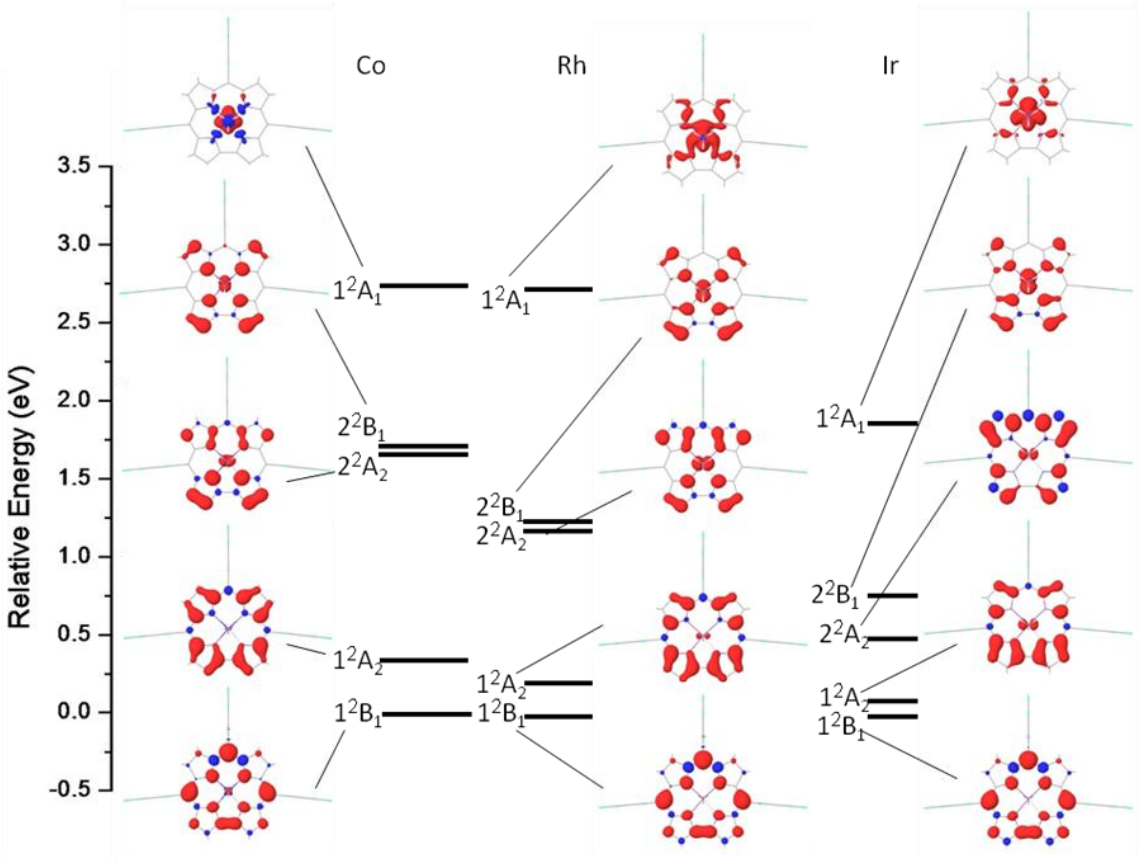

Figure 4-3: Relative energies and spin density surfaces (isovalue = 0.002 a.u.) of $[\mathbf{1}\text{-}\mathbf{M(NH_3)_2}]^+$ (M = Co, Rh, Ir). The calculations were conducted in vacuum by DFT using the 2-ζ valence functions with Hay and Wadt pseudopotentials for the metals and 6-31G** basis set for all the other atoms. The B3LYP functional was employed.

Table 4-3: Spin densities and energies of the excited states of the tfc complexes. The symmetry label of the state is the symmetry of the orbital from which the electron has been ionized. For Rh and Co, other states lying between 3^2B_1 and 1^2A_1 but having the unpaired electron in corrole-based orbitals were omitted in order to include the metal-dominated 1^2A_1. The calculations were conducted in vacuum by DFT using the 2-ζ valence functions with Hay and Wadt pseudopotentials for the metals and 6-31G** basis set for all the other atoms. The B3LYP functional was employed. [a]Energy of the state in question minus that of the lowest energy ionized state of the same compound. [b]Spin given in total unpaired electrons.

$[(tfc)M(NH_3)_2]^+$	**M = Co**		**M = Rh**		**M = Ir**	
State	**Relative energy (eV)[a]**	***Metal spin density*[b]**	**Relative energy (eV) [a]**	***Metal spin density*[b]**	**Relative energy (eV) [a]**	***Metal spin density*[b]**
1^2B_1	0.00	*-0.02*	0.00	*-0.01*	0.00	*-0.01*
1^2A_2	0.67	*0.00*	0.63	*0.02*	0.54	*0.07*
2^2A_2	1.94	*0.08*	1.58	*0.19*	1.21	*0.24*
2^2B_1	2.02	*0.10*	1.62	*0.22*	1.21	*0.35*
3^2B_1	2.33	*-0.01*	2.28	*0.00*	2.27	*0.00*
1^2A_1	3.19	*1.16*	3.19	*0.77*	2.53	*0.91*

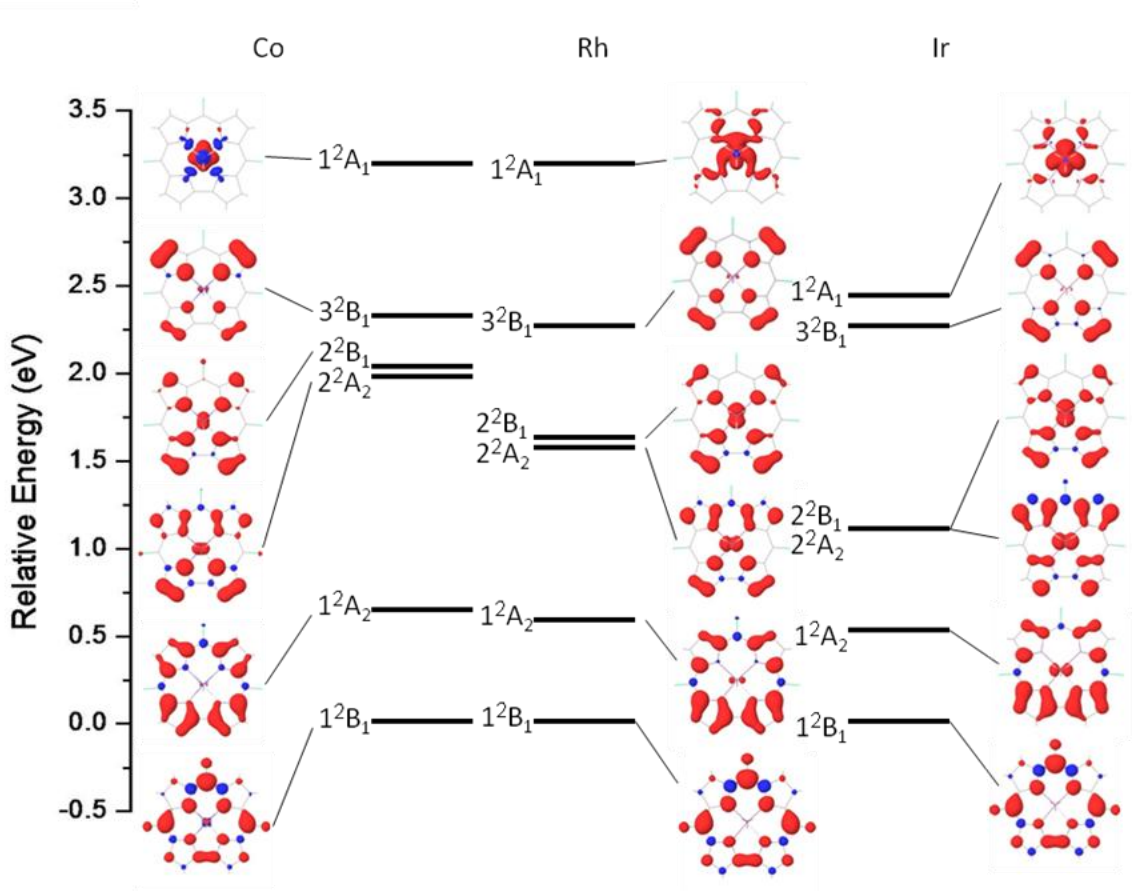

Figure 4-4: Relative energies and spin density surfaces (isovalue = 0.002 a.u.) of $[\mathbf{1f\text{-}M(NH_3)_2}]^+$ (M = Co, Rh, Ir). The calculations were conducted in vacuum by DFT using the 2-ζ valence functions with Hay and Wadt pseudopotentials for the metals and 6-31G** basis set for all the other atoms. The B3LYP functional was employed.

From the energy levels in both the tpfc and the tfc systems, it is apparent that the separation between states decreases in the order Co > Rh > Ir for each corrole system. Also, it is noteworthy that the spin density localized on the metal generally increases in the order Co < Rh < Ir for a given orbital level, except for the high-lying 1^2A_1 state, which occurs in the order Rh < Ir < Co. States classified as 3^2B_1 only appear in the tfc complexes because they are pushed upward in energy when the ligand is tpfc. Figure 4-4 shows that the energy of the 3^2B_1 state relative to the 1^2B_1 state in the three tfc complexes is roughly the same for all three metals.

For a given metal center, the tpfc complex has smaller energy gaps between different states than the tfc complex. An exception is the gap between the nearly degenerate 2^2B_1/ 2^2A_2 states and the adjacent 1^2A_2 state, which is actually greater by around 0.04 eV in the tpfc case due to stabilization of the 1^2A_2 state by the pentafluorophenyl substituents on tpfc. The contraction observed between the lowest two energy states for the different corroles is of a greater order than the difference brought about by changing the metal center for each corrole, presumably because the ground 1^2B_1 state is more effectively stabilized by fluorine than by pentafluorophenyl meso-substituents. [**1-Ir(NH$_3$)$_2$**]$^+$ has the smallest state separations of all compounds under study, such that the energy gap between 1^2B_1 and 1^2A_2 states is only approximately 0.15 eV in vacuum, dropping to 0.10 eV if dichloromethane solvation is added to the model. Solvation with dichloromethane generally decreases the energy gaps between states in the systems examined.

Focusing on the two lowest energy states of [**1-Ir(NH$_3$)$_2$**]$^+$, we separately relaxed the geometry (with C_2 symmetry to allow aryl group rotation) of both the 1^2B_1 and 1^2A_2 states within the continuum solvent employing three functionals: GGA (BP86), hybrid (B3LYP), and meta hybrid (M06). Relaxing the 1^2A_2 state further reduces the splitting, as does solvation as mentioned above. The final $1^2B_1/1^2A_2$ splittings, including solvation and relaxation of the states, are 0.00 eV (BP86), 0.07eV (B3LYP), and 0.03 eV (M06). Thus all three functionals agree that the [**1-Ir(NH$_3$)$_2$**]$^+$ state has two nearly degenerate states: a slightly lower energy corrole-based radical state and a slightly higher energy state (by 0.03–0.10 eV) with mixed metal-corrole character.

The calculated reduction potential of $[\mathbf{1}\text{-}\mathbf{Ir(NH_3)_2}]^{0/+}$ (0.64 V vs. SCE) is in excellent agreement with experimental values for $\mathbf{1}\text{-}\mathbf{Ir(tma)_2}$ and $\mathbf{1}\text{-}\mathbf{Ir(py)_2}$ (0.66 and 0.63 V vs. SCE, respectively) obtained *via* cyclic voltammetry.[12,13] The computed reduction potentials of $[\mathbf{1}\text{-}\mathbf{M(NH_3)_2}]^{0/+}$ are 0.64, 0.67, and 0.56 V vs. SCE for M = Ir, Rh, and Co, respectively.

Discussion

Our DFT calculations point toward a common description of the positively charged (singly oxidized) cobalt, rhodium, and iridium corroles as metal(III) complexes chelated by an oxidized, open-shell macrocycle, with an unpaired electron that resides in a corrole-based B_1 symmetry orbital. For a given metal center, substitution of C_6F_5 for F at the meso positions decreases the energetic difference between the vertical excited states of the cations. This energy gap also is strongly affected by the metal, in the order Co > Rh > Ir. The effect of the metal center and that of the meso-substituents on the state energies of the system are largely decoupled for the rhodium and cobalt complexes. However, in the case of iridium, the electronically excited tfc complex exhibits degenerate states ($2^2B_1/2^2A_2$) that are nondegenerate in the corresponding tpfc complex.

The remarkable effects of meso substituents on the energy levels of the corrole complexes may be rationalized by the following arguments: While pentafluorophenyl is a poorer electron-withdrawing group (EWG) than fluorine by inductive effects,[29] the electron-withdrawing effect of the latter substituent is mitigated by its ability to donate electron density from filled fluorine 2p orbitals into the π-system of the corrole, resulting in an overall greater electron-withdrawing effect of the C_6F_5 substituent on the electronic

structure of the complex. This proposal is supported by the finding that the bonds immediately adjacent to the fluorine atoms in the tfc complexes are shorter than the corresponding bonds in tpfc, but the bonds farther away from the meso substituents are similar in the two corrole scaffolds. Additionally, in vacuum, the sum of atomic charges obtained by Mulliken population analysis on the three meso -CF fragments in [**1f-Ir(NH$_3$)$_2$**]$^+$ is +0.41, while in [**1-Ir(NH$_3$)$_2$**]$^+$, the sum over three meso -CC_6F_5 fragments is -0.32. These values are basis set dependent, and are also affected by solvation, but the charges on the -CF fragments are always more positive than those on the -CC_6F_5 fragments.

The expansion of the energy gaps for the tfc complexes implies that the antibonding interaction between the occupied corrole-π and fluorine-π orbitals destabilizes the $2b_1$ orbital. This in turn stabilizes the 1^2B_1 state relative to excited states that have more metal character. There also is a computed contraction of energy gaps upon moving from Co to Rh to Ir, and the combined effects of having a C_6F_5 meso-substituent and the 5d metal in [**1-M(NH$_3$)$_2$**]$^+$ lead to a situation where the 1^2A_2 state (which has substantial unpaired spin density on the metal atom) is essentially degenerate with the lowest energy $^2B_1$ state when solvation effects are included.

These observations help explain the experimental finding of increased metal character in singly oxidized **1-M(tma)$_2$** and **1-M(py)$_2$** complexes going from Co to Rh to Ir,[12] especially when the effect of spin-orbit coupling, which should stabilize metal-based radicals more in the 5d case than in the lighter metal complexes, is taken into account. Addition of spin-orbit effects into our DFT models is beyond the scope of our current

report, but given that spin-orbit coupling in 5d metals is known to be on the order of 0.5 eV, the 1^2A_2 state of [**1-Ir(NH$_3$)$_2$**]$^+$, which is of mixed metal-corrole character, could easily drop lower in energy than the 1^2B_1 corrole π-cation state. It should be emphasized that the experimental EPR spectra of [**1-Ir(tma)$_2$**]$^+$ and [**1-Ir(py)$_2$**]$^+$ display highly rhombic g-tensors attributable to largely Ir-based SOMOs.[12] A study on the Fe^{II}, Ru^{II}, and Os^{II} complexes of octaethylporphyrin (OEP) by Brown and co-workers similarly found that Ru(OEP)(CO)(thf) is oxidized at the macrocycle while Os(OEP)(CO)(py) is oxidized on the metal.[30] For cobalt and rhodium, on the other hand, the energy difference between the 1^2A_2 and 1^2B_1 states is larger than for iridium and, moreover, spin-orbit effects on their 1^2A_2 states will be much smaller.

The calculated reduction potentials are very similar among the series of [**1-M(NH$_3$)$_2$**]$^{0/+}$ redox pairs. The metal centers have very minor effects on the energy of the corrole-based HOMO of each complex, leading to the computed result that their energies (and therefore their reduction potentials) are the same regardless of the metal center. We had expected that the metal center would perturb the energy levels of the corrole orbitals by providing an altered electric field, and that these differences in the effective electronic shielding by each metal would lead to large changes in the reduction potentials of the complexes. However, we observe fairly minor differences among the computed reduction potentials of the three Group 9 corrole complexes, consistent with experimental data. The computed reduction potential for the Ir case (0.64 V vs. SCE) agrees quite well with experiment (0.63 to 0.66 V vs. SCE). The calculated values for Rh (0.67 V vs. SCE) and Co (0.56 V vs. SCE) are similar to Ir, compared to experimental **1-Rh(py)$_2$** and **1-Co(py)$_2$** potentials of 0.71 and 0.67 V vs. SCE, respectively. These results suggest that corrole-based

orbitals offset any changes to the redox potentials that would be introduced by changing the metal, leading to the conclusion that the ground state wavefunction cannot be metal-centered in the complex cations.

Conclusion

DFT calculations (B3LYP with Poisson-Boltzmann continuum solvation) applied to the series of Group 9 metallocorrole complexes **1-M(NH$_3$)$_2$** (M = Co, Rh, Ir) and the corresponding cations predict a common, ligand-based one-electron oxidation from the corrole HOMO in each case. Wavefunctions for the neutral M^{III} molecules share a HOMO of B_1 symmetry with very small contributions from the metal. The ground state wavefunctions for the cations yield spin densities with little contribution (~ 0.01 electron) from the metals. Calculated reduction potentials (0.64 V, 0.67 V, and 0.56 V vs. SCE for M = Ir, Rh and Co, respectively) are insensitive to the metal within the accuracy of the calculation, and are consistent with the measured reduction potentials of similar Ir(III) corroles (0.63 to 0.66 V vs. SCE).

In the cations, vertical excitation energies to states with significant metal character decrease in the order Co > Rh > Ir, and are negligible in [**1-Ir(NH$_3$)$_2$**]$^+$. Spin-orbit coupling, omitted in the calculations at this level of theory, must mix the low-lying states incorporating Ir d_π character to yield a mixed metal-ligand radical ground state that accords with the experimental EPR spectra of the iridium corrole cations.

Acknowledgements: This work was supported by an NSF Center for Chemical Innovation (CCI Powering the Planet, Grants CHE-0802907 and CHE-0947829), the US-

Israel BSF (Z.G. and H.B.G.), CCSER (Gordon and Betty Moore Foundation), and the Arnold and Mabel Beckman Foundation. S.S.D. was supported from the Overseas Research Fellowship Scheme from the Faculty of Science, University of Hong Kong.

References

(1) Shilov, A. E.; Shul'pin, G. B. *Chem. Rev.* **1997,** *97*, 2879–2932.
(2) Cape, J. L.; Siems, W. F.; Hurst, J. K. *Inorg. Chem.* **2009,** *48*, 8832–8846.
(3) Ringenberg, M. R.; Kokatam, S. L.; Heiden, Z. M.; Rauchfuss, T. B. *J. Am. Chem. Soc.* **2008,** *130*, 788–789.
(4) Han, A.–R.; Jeong, Y. J.; Kang, Y.; Lee, J. Y.; Seo, M. S.; Nam, W. *Chem. Comm.* **2008,** *9*, 1076–1078.
(5) Loew, G. H.; Harris, D. *Chem. Rev.* **2000,** *100*, 407–420.
(6) Green, M. T. *J. Am. Chem. Soc.* **1999,** *121*, 7939–7940.
(7) Shaik, S.; Cohen, S.; Wang, Y.; Chen, H.; Kumar, D.; Thiel, W. *Chem. Rev.* **2010,** *110* , 949–1017.
(8) Aviv–Harel, I.; Gross, Z. *Chem. Eur. J.* **2009,** *15* , 8382–8394.
(9) a) Kadish, K. M.; Shen, J.; Fremond, L.; Chen, P.; El–Ojaimi, M.; Chkounda, M.; Gros, C. P.; Barbe, J.–M.; Ohkubo, K.; Fukuzumi S.; Guilard R. *Inorg. Chem.* **2008,** *47*, 6726–6737. b) Bendix, J.; Dmochowski, I. J.; Gray, H. B.; Mahammed, A.; Simkhovich, L.; Gross, Z. *Angew. Chem., Int. Ed.* **2000,** *39*, 4048–4051.
(10) Gross, Z; Gray, H. B. *Comm. Inorg. Chem.*, **2006**, *27*, 61–72
(11) a) Roos, B. O.; Veryazov, V.; Conradie, J.; Taylor, P. R.; Ghosh, A. *J. Phys. Chem. B.* **2008,** *112*, 14099–14102. b) Zakharieva, O; Schunemann V.; Gerdan M.; Licoccia S.; Cai S.; Walker F. A.; Trautwein A. X. *J. Am. Chem. Soc.* **2002**, *124*, 6636–6648.
(12) Palmer, J. H.; Mahammed, A.; Lancaster, K. M.; Gross, Z.; Gray, H. B. *Inorg. Chem.* **2009,** *48*, 9308–9315.
(13) Palmer, J. H.; Day, M. W.; Wilson, A. D.; Henling, L. M.; Gross, Z.; Gray, H. B. *J. Am. Chem. Soc.* **2008,** *130*, 7786–7787.
(14) Tse, M. K.; Zhang, Z.; Mak, T. C. W.; Chan, K. S. *Chem. Commun.* **1998,** 1199–1200.
(15) Ghosh, A.; Steene, E. *J. Inorg. Biochem.* **2002,** *91*, 423–436.
(16) Jaguar 7.0, release 207; Schrodinger, LLC: New York, **2006**. see Greeley, B. H.; Russo, T. V.; Mainz, D. T.; Friesner, R. A.; Langlois, J–M.; Goddard, W. A., III; Donnelly, R. E. and Ringnalda, M. N. J. Chem. Phys. **1994,** *101*, 4028–4041.
(17) a) Becke, A. D. *Phys. Rev. A.* **1998,** *38*, 3098–3100. b) Lee, C.; Yang, W.; Parr, R. G. *Phys. Rev. B.* **1988,** *37*, 785–789. c) Stephens, P. J.; Devlin, F. J.; Chabalowski, C. F.; Frisch, M. J. *J. Phys. Chem.* **1994,** *98*, 11623–11627.
(18) a) Baik, M.–H.; Friesner, R. A.; *J. Phys. Chem. A.* **2002,** *106*, 7407–7412. b) Chiorescu, I.; Deubel, D. V.; Arion, V. B.; Keppler, B. K. *J. Chem. Theory Comput.* **2008,** *4*, 499–506. c) Roy, L. E.; Jakubikova, E.; Guthrie, M. G.; Batista, E. R. *J. Phys. Chem. A* **2009**, *113*, 6745–6750
(19) Radon, M.; Broclawik, E. *J. Chem. Theory Comput.*, **2007,** *3*, 728–734.
(20) a) Goddard, W.A, III. *Phys. Rev.* **1968**, *174*, 659–662. b) Melius, C.F.; Goddard, W.A, III. *Phys. Rev. A* **1974**, *10*, 1528–1540. c) Melius, C. F.; Olafson, B. D.; Goddard, W. A., III. Chem. Phys. Lett. **1974,** *28*, 457–462.
(21) Hay, P. J.; Wadt, W. R. *J. Chem. Phys.* **1985,** *82*, 299–310.
(22) a) Hehre, W. J.; Ditchfield, R.; Pople, J. A. *J. Chem. Phys.* **1972,** *56*, 2257–2261. b) Hariharan, P. C.; Pople, J. A. *Theor. Chim. Acta* **1973,** *28*, 213–222.
(23) Martin, J. M. L.; Sundermann, A. *J. Chem. Phys*. **2001,** *114*, 3408–3420.
(24) a) Tannor, D. J.; Marten, B.; Murphy, R.; Friesner, R. A.; Sitkoff, D.; Nicholls, A.; Ringnalda, M.; Goddard, W. A., III; Honig, B. *J. Am. Chem. Soc.* **1994**, *116*, 11875–11882. b) Marten, B.; Kim, K.; Cortis, C.; Friesner, R. A.; Murphy, R. B.; Ringnalda, M. N.; Sitkoff, D.; Honig, B. *J. Phys. Chem.* **1996**, *100*, 11775–11788. The Poisson–Boltzmann method is well suited to this application given the absence of extreme, localized electrostatic potentials and opportunities for solvent coordination.
(25) a) Bryantsev, V. S.; Diallo, M. S.; Goddard, W. A., III. *J. Phys. Chem. A*, **2007**, *111*, 4422–4430. b) Nielsen, R. J.; Keith, J. M.; Stoltz, B. M.; Goddard, W. A., III. *J. Am. Chem. Soc.* **2004**, *126*, 7967–7974.
(26) $\Delta G(H^+(1atm) \rightarrow H^+(1M))$ = –264.0 kcal/mol: Tissandier, M. D.; Cowen, K. A.; Feng, W. Y.; Gundlach, E.; Cohen, M. H.; Earhart, A. D.; Coe, J.V.; Tuttle, T. R., Jr. *J. Phys. Chem. A* **1998**, *102*, 7787–7794.

(27) "Electrochemical Series" in *CRC Handbook of Chemistry and Physics, Internet Version **2007**, (87th Edition)*, David R. Lide, ed., Taylor and Francis, Boca Raton, FL.
(28) Ghosh, A.; Wondimagegn, T.; Parusel, A. B. J. *J. Am. Chem. Soc.* **2000**, *122*, 5100–5104.
(29) Hansch, C.; Leo, A.; Taft, R. W. *Chem. Rev.* **1991**, *91*, 165–195.
(30) Brown, G. M.; Hopf, F. R.; Meyer, T. J.; Whitten, D. G. *J. Am. Chem. Soc.* **1975**, *97*, 5385–5390.